Direct Dynamics of an Alkoxy Radical (CH_3O, C_2H_5O, and *i*-C_3H_7O) Reaction with an Oxygen Molecule

Osamu Setokuchi* and Masaru Sato

National Institute of Advanced Industrial Science and Technology (AIST), Onogawa 16-1, Tsukuba 305-8569, Japan

Received: December 31, 2001; In Final Form: April 19, 2002

We calculated the rate constants for an alkoxy radical (CH_3O, C_2H_5O and *i*-C_3H_7O) reaction with an oxygen molecule over a temperature range of 200−1000 K by means of dual-level direct dynamics, based on both the high-level ab initio theory and the variational transition state theory (VTST). We determined the potential energy surfaces at the B3LYP/6-311G(d,p) level and performed single-point calculations at the G2M(RCC1) level to obtain more accurate energies. The calculated rate constants and the temperature dependence are compared with those in the experiment. The improved canonical variational TST rate constants with small curvature tunneling correction agree reasonably well with the experimental rate constants of the $CH_3O + O_2$ and *i*-$C_3H_7O + O_2$ reactions, in which only the ground-state A′ alkoxy radicals react with O_2. In contrast, we suggest that both the ground electronic state A″ and the low-lying excited electronic state A′ ethoxy radicals participate in the reaction of $C_2H_5O + O_2$. The $C_2H_5O + O_2$ reaction rate constant calculated under this assumption is in good agreement with the experimental data. The temperature dependence of the rate constants for these reactions exhibited a non-Arrhenius behavior. It is important to note that the bottleneck of the *i*-$C_3H_7O + O_2$ reaction has a large variational effect and thus can be explained only by employing a theory based on the variational principle.

Introduction

Alkoxy radicals, formed from the OH radical-initiated reaction of hydrocarbons followed by a reaction with O_2 and NO, are key intermediates in the troposphere. The major removal processes of alkoxy radicals involve reactions with O_2 and unimolecular decomposition. The reaction with O_2 for simple lower alkoxy radicals with abstractable hydrogen atoms, $RO + O_2 \rightarrow R_{-H}O + HO_2$ is believed to be more important than unimolecular decomposition. Thus, determination of the rate constants for a CH_3O,[1−3] C_2H_5O,[3−6] and *i*-C_3H_7O[6−8] radical reaction with an oxygen molecule has been the subject of several experimental studies, and the rate constants have recently been reviewed.[9] Two theoretical studies of the $CH_3O + O_2$ reaction mechanism have also recently been conducted.[10,11] Bofill et al. reported that the reaction proceeds by the hydrogen abstraction via a complex caused by a noncovalent O−O bonding interaction[11] rather than an elimination reaction via a trioxy radical.[10] In this paper, we address the direct dynamics for CH_3O, C_2H_5O, and *i*-C_3H_7O radical reactions with an oxygen molecule to investigate the temperature dependence of the rate constants. The alkoxy radicals have three, two, and one abstractable hydrogen atom; dynamics calculations may provide systematic information about the alkoxy radical reaction with an oxygen molecule. To our knowledge, this is the first systematic theoretical study that investigates the rate constants for alkoxy radical reactions with an oxygen molecule. Because most experimental rate constants are limited up to room temperature, it would be useful to observe the behavior of rate constants below room temperature, which is important in the troposphere. For this purpose, we calculated the reaction rate constants with the TST theory and canonical variational theory and compared them with the available experimental data.

Computational Methodology

The geometries at the stationary points were optimized at the B3LYP//6-311G(d,p) level, along with subsequent force constant matrix calculations at the same level. The minimum energy paths (MEP) were calculated using the Hessian matrix at the transition state, in steps of $0.2a_0$ using the Gonzalez-Schlegel IRC algorithm,[12] in which the IRC was calculated at the B3LYP level. The harmonic vibrational frequencies of the generalized normal modes orthogonal to the IRC were calculated at each point on the MEP by diagonalizing the projected force constant matrix.[13] Single-point calculations were performed at the stationary points and each point on the MEP using the G2M-(RCC1) scheme,[14] in which the spin projection for an open-shell system is applied to the Møller−Plesset calculation (MP2 and MP4) in the scheme and any spin contamination arising from the states with spin $(s + 1)$ to $(s + 4)$ is eliminated.[15] The UHF wave functions used in the Møller−Plesset calculation were tested for instability and reoptimized if necessary. Calculations of the RCCSD(T) component in the scheme were performed using the algorithm by Knowles et al.[16] To assess the validity of the IRC calculations at the UB3LYP level, we compared the change in geometrical parameters along the reaction coordinate for the $CH_3O + O_2$ reaction with those at the complete active space self-consistent-field (CASSCF) and ROB3LYP levels. In the CASSCF calculation, 25 electrons were distributed among 16 orbitals and the TZV(2df,2p) basis set[17,18] was used. The calculations based on the B3LYP and MP*n* in the G2M(RCC1) scheme were performed using Gaussian 98 programs,[19] and calculation of the RCCSD(T) level of the theory required MOLPRO 2000 programs.[20] The electronic structure calculations at the CASSCF level were performed using the GAMESS programs.[21] Dual-level variational transition state

10.1021/jp014738u CCC: $22.00
Published on Web 08/09/2002

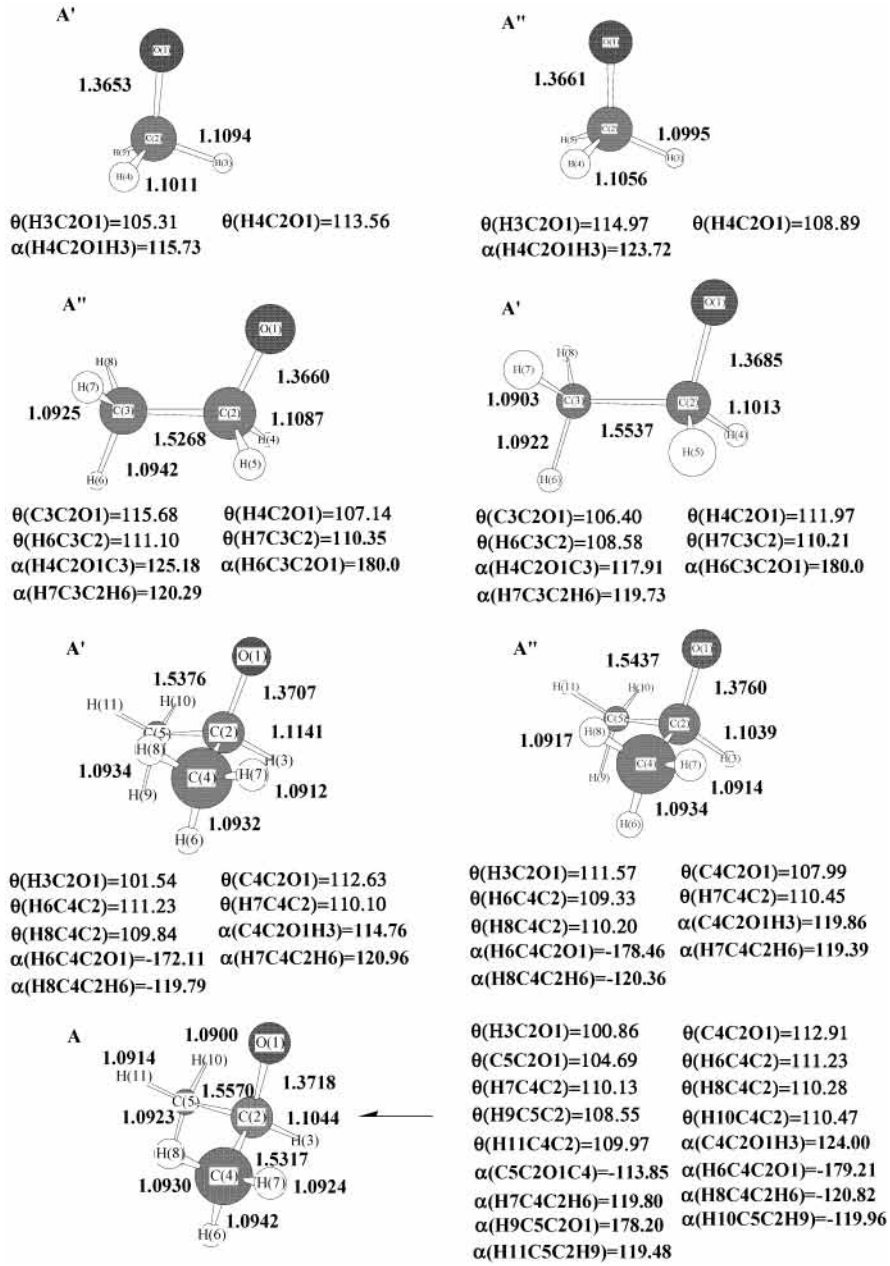

Figure 1. Geometries of CH_3O, C_2H_5O, and *i*-C_3H_7O alkoxy radical at the B3LYP/6-311G(d,p) level. Bond lengths, *R*, are in Å; bond angles, θ, and dihedral angles, α, are in deg.

theory (VTST) calculations, based on the ISPE scheme, were performed with MEP information obtained from electronic structure calculations, wherein ISPE denotes that the higher-level information consists of interpolated single-point energies, that is, G2M(RCC1) energies. In this scheme, we first calculate a converged reaction path at the B3LYP level. A spline under tension is then used to interpolate the difference in the G2M-(RCC1) energy along the MEP at the B3LYP level and the B3LYP energy. The thermal rate constants were calculated using the improved canonical variational theory (ICVT) with small-curvature semiclassical adiabatic ground-state (SCSAG) tunneling contributions.[22,23] The generalized transition state in ICVT is optimized microcanonically for energies up to the microcanonical variational threshold energy and canonically for a higher-energy contribution. The multidimensional semiclassical tunneling correction was calculated using the transmission coefficient obtained based on the small-curvature tunneling (SCT) approximations. These thermal rate constants were calculated using POLYRATE 8.5.1 code.[24]

Results and Discussion

1. Geometries and Energetics. Alkoxy radical geometries at the B3LYP/6-311G(d,p) level are given in Figure 1, and the B3LYP and G2M(RCC1) energies and frequencies for the stationary points are provided in Table 1. The geometries of the methoxy radical and the transition state are identical to those of Jungkamp and Seinfeld.[10] When the ground electronic ^{2}E state of the methoxy radical undergoes the Jahn−Teller effect, the ground-state geometry distorts from C_{3v} to C_s symmetry leading to a nondegenerate ground ^{2}A′ state. The calculation is performed under C_s symmetry, in which the degeneracies are removed by the Jahn−Teller effect. Ethoxy and *i*-propoxy radicals have only a plane of symmetry, that is, the C_s symmetry plane. Under C_s symmetry, the ground electronic states of methoxy, ethoxy, and *i*-propoxy radicals have A′, A″, and A′ symmetry. Experimental[25−27] and theoretical[28] studies have demonstrated that the ground electronic state of the ethoxy radical has A″ symmetry. The low-lying excited A′ state of an

TABLE 1: Energies (au) and Vibrational Frequencies (cm^{-1}) at the Stationary Points

species	B3LYP[a]	G2M(RCC1)[a]	frequency ν[b]
CH_3O (A′) + O_2	−265.450 913	−265.066 576	2996, 2956, 2890, 1518, 1371, 1361, 1108, 964, 772
	−265.410 873	−265.026 536	
CH_3O-O_2 (complex)	−265.452 366	−265.063 272	2996, 2953, 2878, 1632, 1516, 1374, 1365, 1112, 967,
	−265.411 153	−265.030 527	786, 142, 102, 98, 56, 54
CH_3O-O_2 (TS)	−265.441 607	−265.063 272	2962, 2892, 1671, 1548, 1504, 1360, 1254, 1235,
	−265.401 148	−265.022 814	1111, 703, 565, 488, 245, 213, 1045*i*
C_2H_5O (A″) + O_2	−304.781 862	−304.325 696	3107, 3097, 3030, 2892, 2888, 1496, 1484, 1411,
	−304.713 831	−304.257 665	1391, 1342, 1241, 1098, 1069, 886, 873, 433,
			310, 169
C_2H_5O (A′) + O_2	−304.780 004	−304.324 923	3133, 3123, 3045, 2978, 2940, 1542, 1502, 1471,
	−304.710 550	−304.255 468	1386, 1306, 1257, 1132, 969, 929, 899, 590,
			383, 259
$C_2H_5O-O_2$ (complex)	−304.783 340	−304.330 623	3107, 3097, 3030, 2895, 2887, 1631, 1496, 1485,
	−304.714 049	−304.261 332	1411, 1391, 1349, 1243, 1098, 1067, 895, 886,
			463, 434, 229, 130, 87, 64, 43, 13
$C_2H_5O-O_2$ (TS)	−304.773 739	−304.324 299	3116, 3097, 3031, 2880, 1691, 1526, 1490, 1479,
	−304.705 449	−304.256 009	1405, 1393, 1295, 1248, 1096, 1086, 910, 843,
			682, 527, 469, 224, 194, 161, 134, 976*i*
i-C_3H_7O (A′) + O_2	−344.110 628	−343.585 699	3117, 3115, 3101, 3095, 3035, 3028, 2831, 1504,
	−344.013 423	−343.488 494	1494, 1486, 1479, 1406, 1383, 1252, 1198,
			1158, 1084, 1047, 975, 912, 891, 802, 449,
			401, 356, 233, 193
i-C_3H_7O (A) + O_2	−344.110 228	−343.586 119	3131, 3118, 3105, 3095, 3041, 3027, 2921, 1509,
	−344.012 636	−343.488 527	1490, 1482, 1470, 1402, 1378, 1356, 1267,
			1154, 1087, 1038, 935, 924, 880, 807, 417,
			380, 343, 293, 198
i-$C_3H_7O-O_2$ (complex)	−344.112 067	−343.592 467	3116, 3115, 3101, 3095, 3034, 3028, 2822, 1633,
	−344.014 121	−343.494 522	1504, 1494, 1486, 1479, 1408, 1385, 1261, 1200,
			1163, 1088, 1051, 975, 912, 897, 803, 456, 403,
			355, 233, 194, 111, 68, 46, 44, 31
i-$C_3H_7O-O_2$ (TS)	−343.103 721	−343.585 257	3124, 3122, 3099, 3094, 3032, 3028, 1697, 1525,
	−344.007 832	−343.489 368	1494, 1489, 1480, 1474, 1398, 1379, 1336,
			1159, 1157, 1083, 1055, 941, 890, 794, 692,
			543, 476, 401, 307, 216, 182, 178, 136,
			100, 824*i*

[a] Upper and lower entries represent electronic energies and energies involving zero-point energy, respectively. [b] *i* represents imaginary frequency. B3LYP = −150.361 052; G2M = −150.154 424; ν = 1641 for O_2 molecule.

ethoxy radical has a stable minimum and is 482 cm^{-1} higher than the ground state of the A″ state at the G2M(RCC1) level, which agrees reasonably well with a recent observation (355 cm^{-1}) by photoelectron spectroscopy.[26] The A″ geometry of methoxy and *i*-propoxy radicals has an imaginary vibrational frequency, and thus the local minimum does not exist in the A″ state for alkoxy radicals. A stationary point with C1 symmetry, which originates from A″ symmetry, was found instead for *i*-propoxy radicals, as shown in Figure 1.

Bofill et al.[11] demonstrated that the reaction proceeds with a direct hydrogen abstraction mechanism via a prereaction complex, RO + O_2 → complex → TS → $R_{-H}O$ + HO_2. The complex and transition-state geometries at the B3LYP/6-311G(d,p) level are shown in the left and right sides of Figure 2. The structural differences in the TS and the complex among three reactions can be found in the internuclear distance, *R*(O(2)−O(3)). The *R*(O(2)−O(3)) distances in the complex are 2.7399, 2.6882, and 2.8525 Å for CH_3O + O_2, C_2H_5O + O_2, and *i*-C_3H_7O + O_2. The distance depends on the electronic energies of the complex relative to the reactant at the B3LYP/6-311G(d,p) level; they were −0.912 kcal/mol for CH_3O + O_2, −0.927 kcal/mol for C_2H_5O + O_2, and −0.903 kcal/mol for *i*-C_3H_7O + O_2. However, because the order of binding energies is reversed at the G2M(RCC1) level, it is unclear why a C_2H_5O + O_2 complex gives the shortest *R*(O(2)−O(3)) distance. Bofill et al. reported the interaction results in a noncovalent interaction between O(2) and O(3) atoms,[11] in which the forming π character of an alkoxy radical CO bond with reaction progress interacts with an in-plane p orbital on an O(2) atom, and the CO bond length of the complex and the TS is shortened compared with the alkoxy radical CO bond. However, only the CO bond length of the C_2H_5O + O_2 complex is slightly stretched upon complex formation. The short *R*(O(2)−O(3)) distance of a C_2H_5O + O_2 complex accentuates the long internuclear distance between an abstractable hydrogen atom and the terminal oxygen atom, *R*(H(5)−O(1)). The stabilization energies at 0 K of the complexes were −2.5, −2.3, and −3.7 kcal/mol at the G2M(RCC1) level (see Table 1). A more precise calculation of the stabilization energy of a complex may require correction of the basis set superposition error. No correction is required here, because only the energetics around TS ($-1.5 < s < 1.5$ $amu^{1/2}$ bohr) are considered in this dynamics calculation. The *R*(O(2)−O(3)) distances at the transition state increase in the order of CH_3O + O_2 (2.1186 Å), C_2H_5O + O_2 (2.1811 Å), and *i*-C_3H_7O + O_2 (2.2507 Å). Figure 3 depicts the change in the *R*(O(2)−O(3)) nuclear distance along the reaction coordinate based on the IRC calculation, where $s = -\infty$ corresponds to the reactants. O(2) and O(3) can be finally separated when the IRC calculation is followed toward the reactant. However, the minimum *R*(O(2)−O(3)) distance is located at different *s* values among the three reactions. The minimum is located at $s = -1.0$ $amu^{1/2}$ bohr for CH_3O + O_2, $s = -0.04$ $amu^{1/2}$ bohr for C_2H_5O + O_2, and $s = +0.2$ $amu^{1/2}$ bohr for *i*-C_3H_7O + O_2. A previous IRC calculation[10] led to a trioxy radical as the reactant, which indicates a decrease in the *R*(O(2)−O(3)) distance toward $s = -\infty$.

We compared the change in geometrical parameters along the reaction coordinate at the UB3LYP level with that at the CASSCF and ROB3LYP level for the CH_3O + O_2 reaction. Figure 4 shows the change in *R*(O(2)−O(3)) for the CH_3O +

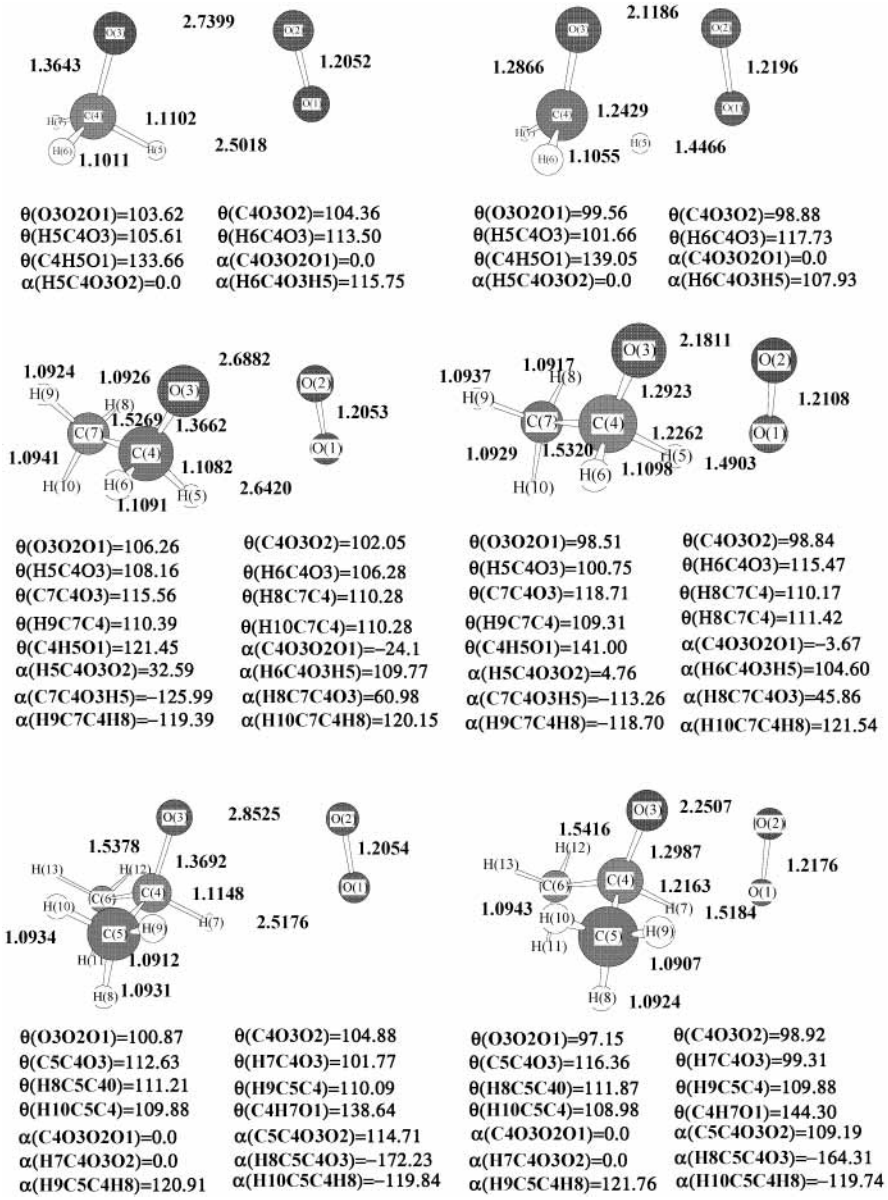

Figure 2. Geometries of complex (left) and transition state (right) at the B3LYP/6-311G(d,p) level. Bond lengths, *R*, are in Å; bond angles, θ, and dihedral angles, α, are in deg.

O_2 reaction along the IRC. The *R*(O(2)−O(3)) at the UB3LYP and CASSCF level decreases slightly, but the *R*(O(2)−O(3)) begins to increase at $s = -1.0$ in case of the B3LYP level and at $s = -2.5$ in case of the CASSCF level, when the IRC is followed in the direction of the reactants. Thus, the change in *R*(O(2)−O(3)) at the UB3LYP level is similar to that at the CASSCF level. In contrast, *R*(O(2)−O(3)) at the ROB3LYP level decreases, incorrectly leading to a trioxy radical such as a previous IRC calculation,[10] when the IRC is followed in the direction of the reactants. Changes in the other geometrical parameters *R*(C(4)−H(5)), *R*(O(1)−H(5)), and θ(C(4)H(5)-O(1)) along the IRC are shown in Figures S1, S2, and S3 as Supporting Information. The IRC behavior at the UB3LYP level qualitatively agrees with that at the CASSCF level. Comparison between the B3LYP potential energy surface and G2M(RCC1) potential energy surface is shown in Figure S4. The similarity of the shape suggests that the IRC calculation at the B3LYP level is a zero-order approximation for the G2M(RCC1) potential energy surface, although the UB3LYP energy barrier height is several kcal/mol higher than the G2M(RCC1) one. A spin expectation $\langle S^2 \rangle$ value at the TS for the $CH_3O + O_2$ reaction

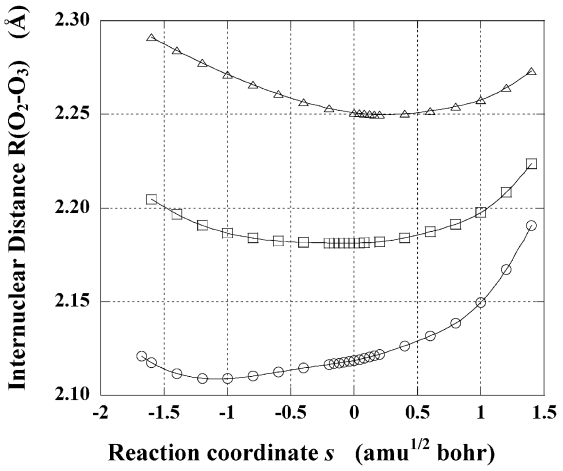

Figure 3. Change in internuclear distance *R*(O(2)−O(3)) along intrinsic reaction coordinate at the B3LYP/6−311G(d,p) level: (○) $CH_3O + O_2$; (□) $C_2H_5O + O_2$; (△) *i*-$C_3H_7O + O_2$.

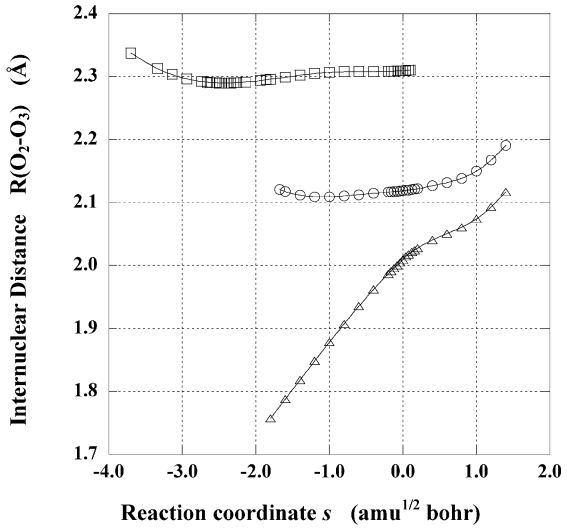

Figure 4. Change in R(O(2)−O(3)) along intrinsic reaction coordinate for the $CH_3O + O_2$ reaction: (○) UB3LYP/6-311G(d,p); (□) CASSCF/TZV(2df,2p); (△) ROB3LYP/6-311G(d,p).

is 1.654 for the UHF/6-311G(d,p) wave function, whereas the UB3LYP/6-311G(d,p) value is 0.895. If the transition-state geometry is optimized at the high level of theory based on an UHF wave function, such as the QCISD or CCSD level, it will suffer a severe spin contamination. Thus, in this regard, a UB3LYP geometry optimization is more favorable than a high-level of theory based on an UHF wave function. Therefore, the use of the B3LYP theory to determine the TS geometries and the IRC for the RO + O_2 reactions seems appropriate.

The difference in the transition-state geometries among the three reactions also appears in the breaking bond, R(C(4)−H), and making bond, R(O(1)−H). To investigate whether the TS structures of the three RO + O_2 reactions conform to Hammond's postulate,[29] which predicts the transition-state structure of a reaction, we considered the relative changes in the making and breaking bond lengths, R_b, as functions of the barrier height ratio, $R_v = V^{\ddagger}_f/(V^{\ddagger}_f + V^{\ddagger}_r)$ according to Truong and Truhlar's definition,[30] wherein $V^{\ddagger}_f$ and $V^{\ddagger}_r$ are the classical forward and reverse barrier heights. R_b is represented by the formula $[(r_1 - r_{1,eq})/r_{1,eq}]/[(r_1 - r_{1,eq})/r_{1,eq} + (r_2 - r_{2,eq})/r_{2,eq}]$, where r_1 and $r_{1,eq}$ are the breaking C−H bond lengths at the transition state and the C−H bond lengths of the alkoxy radical and r_2 and $r_{2,eq}$ are the making O−H bond lengths at the transition state and the O−H bond lengths of the HO_2 radical. These are plotted in Figure 5. According to Hammond's postulate, the TS should be more reactant-like than product-like for an exothermic reaction. These reactions appear to conform to Hammond's postulate, and thus the transition state of the secondary alkoxy radical reaction (i-$C_3H_7O + O_2$) is more reactant-like than that of the primary alkoxy radical reaction ($C_2H_5O + O_2$).

2. Potential Energy Profile Along the Minimum Energy Path. Figure 6 shows the potential energy, V_{MEP} (top), and adiabatic ground-state potential energy, V_a^G (bottom), at the G2M(RCC1) level along the IRC obtained at the B3LYP//6-311G(d,p) level, where $V_a^G = V_{MEP} + \Delta ZPE$, the value of s is the arc length of the IRC from the TS in the unit of amu$^{1/2}$ bohr, and $s < 0.0$ and $s > 0.0$ correspond to the reactant and product regions. The V_{MEP} and V_a^G energies are taken as relative to reactant, which gives an energy of zero. The maximum energy locations of the potential energy surface at the G2M(RCC1) level shift slightly from $s = 0$ toward the products side; that is, $s = +0.12$, $+0.12$, and $+0.04$ amu$^{1/2}$ bohr for $CH_3O + O_2$, $C_2H_5O + O_2$, and i-$C_3H_7O + O_2$. Because the magnitude of the shift is of the same order in the three reactions, the degree of dynamical electron correlation at the G2M(RCC1) level,

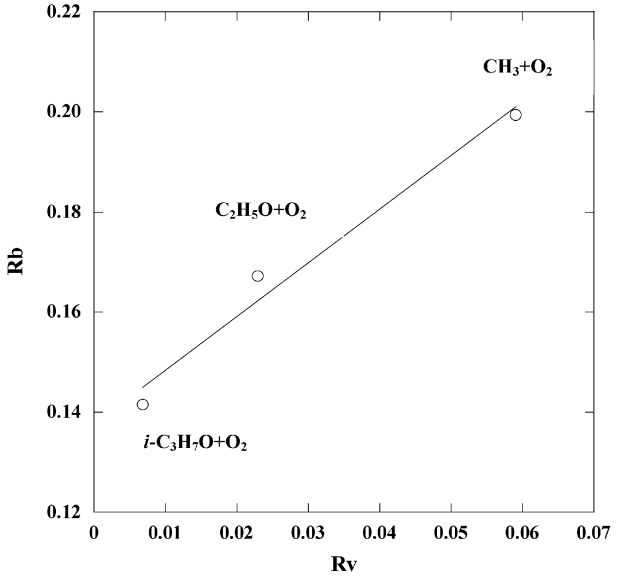

Figure 5. Plot of R_b vs R_v. $R_b = [(r_1 - r_{1,eq})/r_{1,eq}]/[(r_1 - r_{1,eq})/r_{1eq} + (r_2 - r_{2,eq})/r_{2,eq}]$, where r_1 and $r_{1,eq}$ are the breaking C−H bond lengths at the transition state and the C−H bond lengths of the alkoxy radical, and r_2 and $r_{2,eq}$ are the making O−H bond lengths at the transition state and O−H bond lengths of (0.9755 Å) of the HO_2 radical. $R_v = V^{\ddagger}_f/(V^{\ddagger}_f + V^{\ddagger}_r)$, where $V^{\ddagger}_f$ and $V^{\ddagger}_r$ are the classical forward and reverse barrier heights in kcal/mol. $V^{\ddagger}_f = 2.07$ and $V^{\ddagger}_r = 33.06$ for the $CH_3O + O_2$ reaction; $V^{\ddagger}_f = 0.88$ and $V^{\ddagger}_r = 37.37$ for $C_2H_5O + O_2$; $V^{\ddagger}_f = 0.28$ and $V^{\ddagger}_r = 40.60$ for i-$C_3H_7O + O_2$.

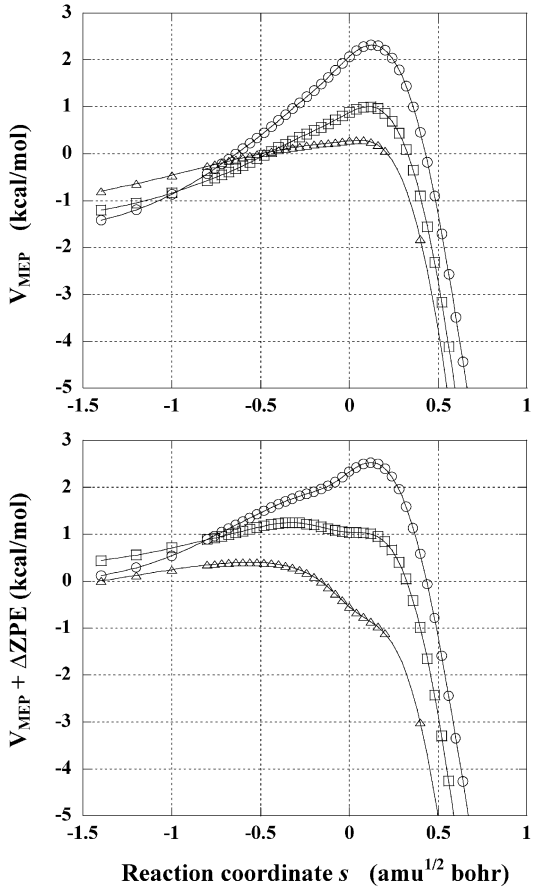

Figure 6. Relative energy along the intrinsic reaction coordinate at the G2M(RCC1) level: (○) $CH_3O + O_2$; (□) $C_2H_5O + O_2$; (△) i-$C_3H_7O + O_2$.

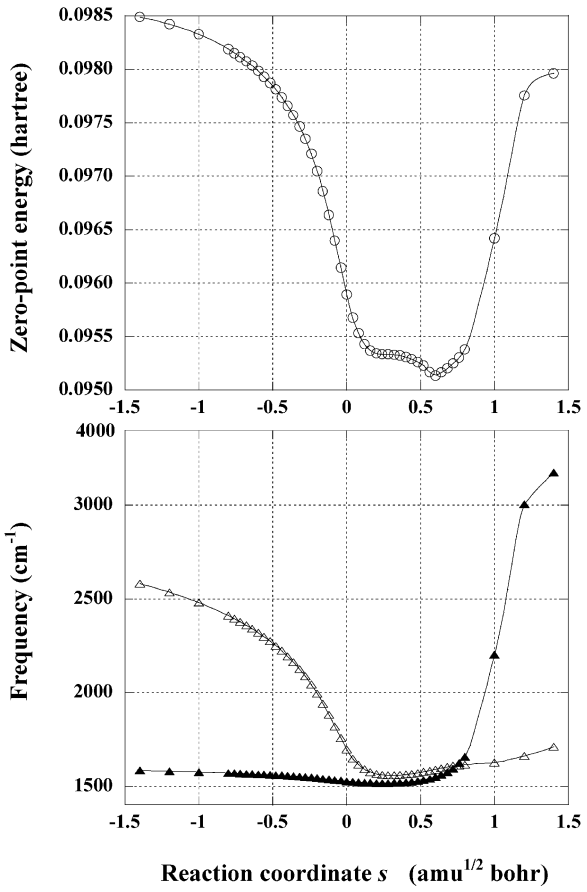

Figure 7. Change in zero-point energy (top) and vibrational frequency (bottom) along intrinsic reaction coordinate for *i*-$C_3H_7O + O_2$ reaction: (△) C−H stretch mode and C−O stretch mode; (▲) O−O stretch mode and H−O stretch mode.

which is not taken into account at the B3LYP/6-311G(d,p) level, is nearly constant for the three reactions. In contrast, the maximum energy locations of the adiabatic potential energy surface shift toward the reactants side, that is, $s = -0.3109$ and -0.5506 amu$^{1/2}$ bohr for the $C_2H_5O + O_2$ and *i*-$C_3H_7O + O_2$ reactions, though the *s* value for $CH_3O + O_2$ remains at 0.127 amu$^{1/2}$ bohr. Thus, the adiabatic potential energy maximum of the secondary alkoxy radical reaction changes significantly from the V_{MEP} maximum. If we take the energy at $s = 0$ for the potential energy barrier height, such as in the treatment of the conventional TST theory and the zero-order interpolated approximation to the zero-curvature vibrationally adiabatic ground-state model, the calculated activation energy will not reproduce the experimental data.

Use of the formula $E_a = \Delta E^* + RT = V^* + \Delta ZPE + \Delta E(T) + RT$ as a simple estimation of the activation energy[31] yields $E_a = 2.6$, 1.4, and -0.8 kcal/mol at $T = 298$ K for $CH_3O + O_2$, $C_2H_5O + O_2$, and *i*-$C_3H_7O + O_2$. A real-gas approximation is used here, and V^* and $\Delta E(T)$ represent the potential barrier height and thermal energy correction. Accordingly, the simple TST theory will incorrectly give a negative activation energy for an *i*-$C_3H_7O + O_2$ reaction (see Figure 11), contrary to the experimental positive activation energy.[6−8] Thus, the rate constants for an *i*-$C_3H_7O + O_2$ reaction should be determined so as to maximize the generalized free energy change, that is, variationally.

The change in zero-point energy and two active generalized vibrational modes along the IRC for an *i*-$C_3H_7O + O_2$ reaction are shown, respectively, at the top and bottom of Figure 7. The zero-point energy decreases as the reaction proceeds from the reactant to the transition state. The minimum zero-point energy is located near $s = 0.5$, which is at the product side beyond TS. The decrease is caused mainly by the decrease in frequency of the breaking bond C−H stretch mode, which correlates with the C═O stretch mode of an acetone product. In contrast, the increase in the zero-point energy on the products side is caused mainly by an increase in the frequency of the making bond H−O stretch mode, which correlates with the O−O stretch mode of an oxygen molecule. Thus, the change in frequency of these active modes influences the change in the zero-point energy. This characteristic applies also to methoxy and ethoxy radical reactions. However, the V_{MEP} of the $CH_3O_2 + O_2$ reaction is steep enough to compensate for vibrational changes, resulting in a negligible variational effect. Because the *i*-$C_3H_7O + O_2$ reaction has a low potential barrier, which may be caused by production of a more stable complex or reduced breaking C−H bond strength, a decrease in the C−H stretch mode frequency of around $s = 0$ results in a remarkable change in the shape of the V_a^G, different from that of V_{MEP}, especially near TS. A similar significant variational effect for a secondary H abstraction has been found on the reaction of the secondary haloethane with an OH radical.[32]

3. Dynamics Calculation. We will first investigate which electronic state of an alkoxy radical can participate in the reaction based on the molecular orbital configuration. Figure 8 shows p-π molecular orbitals localized on oxygen atoms of a TS or a complex, in which the molecular orbital based on the UB3LYP wave function on an O(3) atom of an alkoxy radical and an O(2) atom of an oxygen molecule are shown; the two atoms are above the plane. The first molecular orbital (I) is doubly occupied. The spin doublet state of the reaction system involves UHF orbitals, which consist of a β spin orbital (II) and two α spin orbitals (III and IV). The β spin molecular orbital electron on an O(3) atom (II) interacts noncovalently with an α spin orbital (IV) electron on an O(2) atom. These two orbitals exist in the plane of the C−H bond and oxygen molecules for $CH_3O + O_2$ and *i*-$C_3H_7O + O_2$ reactions with C_s symmetry. We can relate the singly occupied β spin orbital (II) to the singly occupied orbital of the methoxy and *i*-propoxy radicals. Because the singly occupied orbitals are in the symmetry plane represented by the broken line of alkoxy radicals, the electronic state of the reactant methoxy and *i*-propoxy radicals is the A′ state. In contrast, the orbital does not exist in the symmetry plane of the ethoxy radical for an ethoxy radical reaction. We may regard the orbital as one of the hybrid orbitals formed between orbitals in-plane and perpendicular to the symmetry plane; that is, the A′ symmetry p orbital and A″ symmetry p orbital of the ethoxy radical, where the other orbital corresponds to the doubly occupied orbital (I). The occurrence of such a hybrid orbital may be caused by mixing of the A″ ground state and A′ low-lying excited state. The molecular orbital and symmetry consideration of the complex and the TS for *i*-$C_3H_7O + O_2$ reaction with C_s symmetry reveals that the participating reactant *i*-propoxy radical state is an A′ state rather than an A state with C1 symmetry (see Figure 1). Thus, only the electronic ground A′ state methoxy and *i*-propoxy radicals participate in $CH_3O + O_2$ and *i*-$C_3H_7O + O_2$ reactions, but both A″ and A′ electronic states may participate in a $C_2H_5O + O_2$ reaction. The validity of this assumption is examined in the dynamics calculation below.

Figures 9−11 show plots of the logarithm of the rate constant vs the reciprocal absolute temperature, ln(*k*) vs 1/*T*. The calculated ICVT rate constants with a small-curvature tunneling

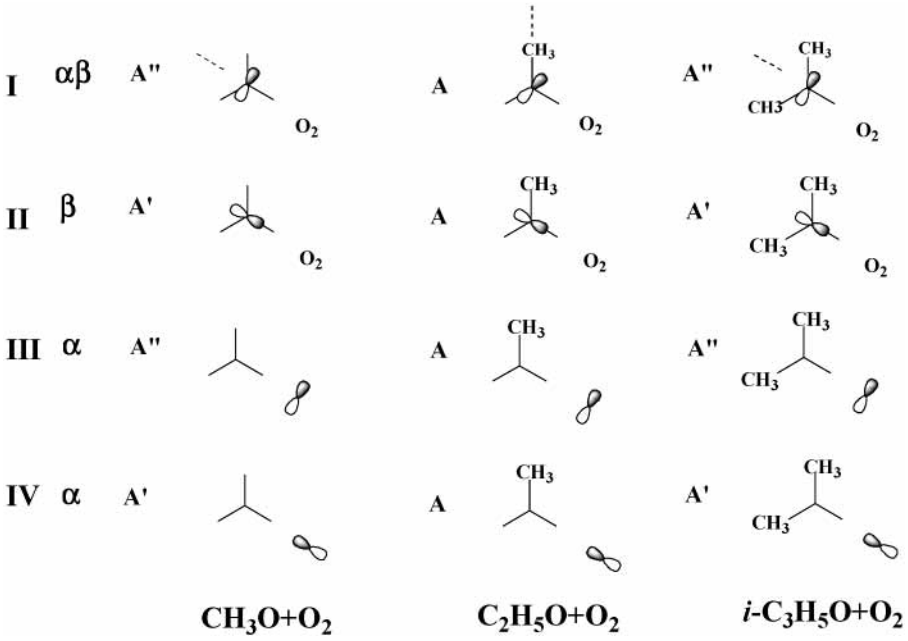

Figure 8. Molecular orbitals of the TS or complex of RO + O_2 reaction. Only p−π occupied UHF spin orbitals on O(2) and O(3) oxygen atoms are shown with the symmetry. Broken lines represent the symmetry planes of alkoxy radicals.

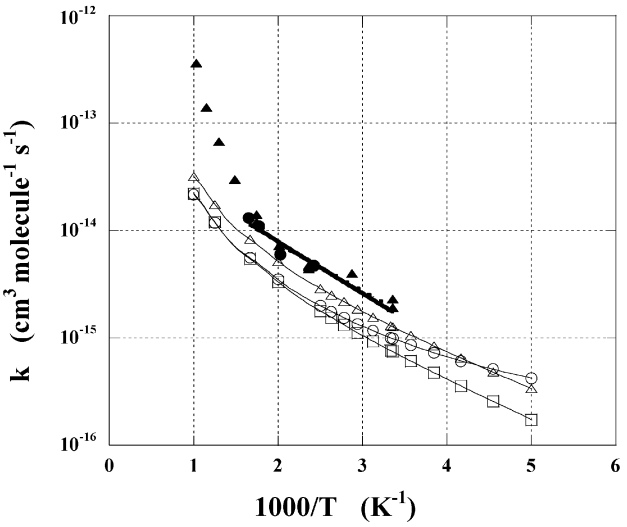

Figure 9. Arrhenius plots of the calculated and experimental rate constants for the $CH_3O + O_2$ reaction: (○) ICVT/SCT; (□) GTST/W; (△) TST/W; (—) ref 9; (···) ref 1; (●) ref 3; (▲) ref 2.

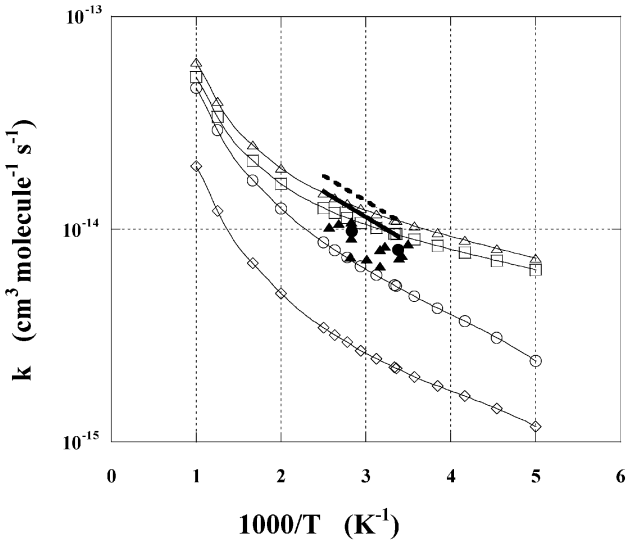

Figure 10. Arrhenius plots of the calculated and experimental rate constants for the $C_2H_5O + O_2$ reaction: (○) ICVT/SCT; (□) GTST/W; (△) TST/W; (—) ref 9; (···) ref 4; (●) ref 3; (▲) ref 6; (◊) ICVT/SCT-2. ICVT/SCT-1 is calculated with contributions from both the ground state and low-lying excited state ethoxy radical, as well as GTST/W and TST/W, while ICVT/SCT-2 is calculated with only contribution from the ground-state ethoxy radical.

correction (ICVT/SCT) and the conventional TST rate constants with a Wigner tunneling correction (GTST/W and TST/W) are compared with available experimental ones, where GTST indicates the generalized TST rate constant at the maximum V_{MEP} at the G2M(RCC1) level, as shown in Figure 6, and TST represents the conventional rate constant at $s = 0$, that is, TS at the B3LYP/6-311G(d,p) level. The GTST/W and TST/W rate constants are higher than those of ICVT/SCT. The TST rate for the $CH_3O + O_2$ and $C_2H_5O + O_2$ reactions may appear to be in good agreement with the experimental data, but the TST rate constants are significantly overestimated for the i-$C_3H_7O + O_2$ reaction and lead to an incorrect temperature dependence at low temperatures. As shown in Figure 6, the maximum V_a^G value for $CH_3O + O_2$ and $C_2H_5O + O_2$ reactions differs slightly from the V_a^G value at $s = 0$ and at the maximum V_{MEP} and thus may appear to give a reasonable value. In contrast, the maximum V_a^G value for i-$C_3H_7O + O_2$ reaction differs significantly from the V_a^G value at $s = 0$ and at the maximum V_{MEP}. This indicates that the bottleneck of the secondary alkoxy radical reaction has a large variational effect caused by the active vibrational mode. We can see the two IVCT/SCT rate constants (ICVT/SCT-1 and ICVT/SCT-2) in Figure 10, in which the ICVT/SCT-2 rate constant is calculated under the assumption that only the A″ ground-state ethoxy radical reacts with the oxygen molecule, while the ICVT/SCT-1 rate constant is calculated with contributions from both the A″ ground state and A′ low-lying excited state, as well as GTST/W and TST/W. If the population of A″ and A′ electronic state ethoxy radical molecules is assumed to be in a thermal Boltzmann distribution, the total rate constant in the ICVT/SCT-1 calculation will be expressed by $k_{ICVT/SCT-1} = w_{A''}k_{A''} + w_{A'}k_{A'}$, where $k_{A''}$ (= $k_{ICVT/SCT-2}$) and $k_{A'}$ are the reaction rate constants of the A″ and A′ electronic state ethoxy

TABLE 2: Calculated ICVT and ICVT/SCT Rate Constants (cm^3 $molecule^{-1}$ s^{-1})[a]

	$CH_3O + O_2$ reaction		$C_2H_5O + O_2$ reaction					i-$C_3H_7O + O_2$ reaction	
T (K)	ICVT	ICVT/SCT	ICVT (A″)	ICVT/SCT (A″)	ICVT (A′)	ICVT/SCT′ (A′)	$w_{A''}$[b]	ICVT	ICVT/SCT
200	5.2 (−17)	4.2 (−16)	6.3 (−16)	1.2 (−15)	3.1 (−14)	3.1 (−14)	0.958	3.6 (−15)	4.6 (−15)
220	8.7 (−17)	5.1 (−16)	8.5 (−16)	1.4 (−15)	3.1 (−14)	3.1 (−14)	0.944	4.2 (−15)	5.2 (−15)
240	1.4 (−16)	6.1 (−16)	1.1 (−15)	1.6 (−15)	3.0 (−14)	3.0 (−14)	0.927	4.8 (−15)	5.8 (−15)
260	2.0 (−16)	7.3 (−16)	1.3 (−15)	1.8 (−15)	2.9 (−14)	2.9 (−14)	0.910	5.5 (−15)	6.4 (−15)
280	2.8 (−16)	8.6 (−16)	1.5 (−15)	2.0 (−15)	2.8 (−14)	2.8 (−14)	0.893	6.2 (−15)	7.1 (−15)
300	3.6 (−16)	9.9 (−16)	1.7 (−15)	2.2 (−15)	2.8 (−14)	2.8 (−14)	0.877	7.0 (−15)	7.8 (−15)
320	3.7 (−16)	1.0 (−15)	1.9 (−15)	2.5 (−15)	2.8 (−14)	2.8 (−14)	0.860	7.7 (−15)	8.6 (−15)
340	4.8 (−16)	1.2 (−15)	2.2 (−15)	2.7 (−15)	2.8 (−14)	2.8 (−14)	0.845	8.6 (−15)	9.4 (−15)
360	6.1 (−16)	1.3 (−15)	2.4 (−15)	2.9 (−15)	2.9 (−14)	2.9 (−14)	0.830	9.4 (−15)	1.0 (−14)
380	7.6 (−16)	1.5 (−15)	2.7 (−15)	3.2 (−15)	2.9 (−14)	2.9 (−14)	0.816	1.0 (−14)	1.1 (−14)
400	9.3 (−16)	1.8 (−15)	2.9 (−15)	3.4 (−15)	3.0 (−14)	3.0 (−14)	0.802	1.1 (−14)	1.2 (−14)

[a] Values in parentheses are power terms. [b] Population of A″ ground state for ethoxy radical, $w_{A''} = N_{A''}/(N_{A''} + N_{A'})$.

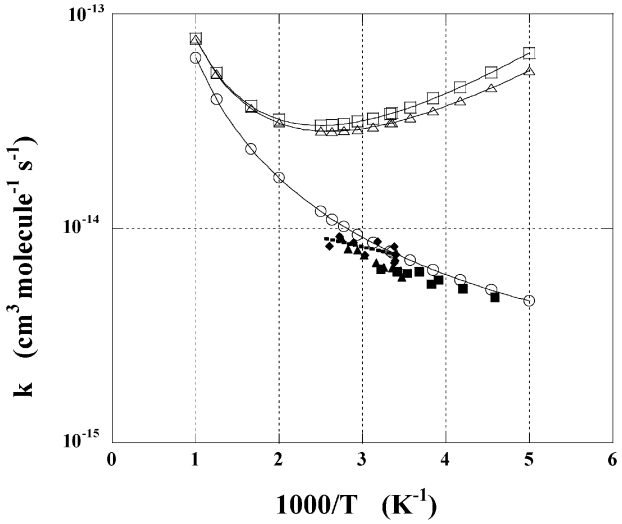

Figure 11. Arrhenius plots of the calculated and experimental rate constants for the i-$C_3H_7O + O_2$ reaction: (○) ICVT/SCT; (□) GTST/W; (△) TST/W; (•••) ref 9; (■) ref 8; (♦) ref 7; (▲) ref 6.

radical molecules, and $w_{A''}$ and $w_{A'}$ are the thermal populations of the A″ and A′ states. The temperature dependence of the population is summarized in Table 2.

A recent study[6] demonstrated that rate constants for an ethoxy radical reaction are somewhat smaller than the recommended value.[9] Even if this is so, the ICVT/SCT-2 rate constant at 298 K still underestimates the experimental value by a factor of 4. However, the ICVT/SCT-1 rate constant at 298 K agrees within a factor of 1.5 because of a large contribution from an A′ excited-state ethoxy radical reaction. $C_2H_5O + O_2$ reaction rate constants have been experimentally measured by laser-induced fluorescence based on the $\tilde{B}A' \leftarrow \tilde{X}A''$ transition. However, if we assume a fast equilibrium between the A″ and A′ electronic state molecules of an ethoxy radical or if these two electronic states are strongly mixed,[26] the apparent reaction rate will be presented as the sum of the contribution from the A″ ground state and the A′ excited state. Symmetry lowering upon complex formation may make the mixing of the two electronic states accessible. Hence, we suggest that the total rate constant ICVT/SCT-1 may be compared with the experimental rate constants. An ICVT/SCT-1 rate constant determined under such an assumption slightly underestimates the experimental data. The degree of underestimation decreases somewhat as the number of methyl substitutions for alkoxy radicals increases.

It is interesting that the calculated ICVT/SCT rate constants for an i-$C_3H_7O + O_2$ reaction are in good agreement with the experimental data, particularly because only recent experimental data[8] is available for low temperatures, below room temperature; Atkinson et al.[9] indicated that the previously reported temperature dependence of the rate constant required confirmation. Canonical variational TST (CVT/SCT) rate constants also give rate constants identical to the ICVT/SCT rate constant for a $CH_3O + O_2$ reaction. However, the transmission coefficient for $C_2H_5O + O_2$ and i-$C_3H_7O + O_2$ gives slightly different values between CVT/SCT and ICVT/SCT rate constants because of the complicated profiles of V_a^G (see $V_{MEP} + \Delta ZPE$ in Figure 6). Therefore, we adopt the more accurate ICVT/SCT rate constants, which are calculated microcanonically (the energy-dependent rate constant) up to the microcanonical variational threshold energy, for the alkoxy radical reactions.

Curvature is often observed in plots of the logarithm of the rate constant vs the reciprocal absolute temperature, ln(k) vs 1/T, which is non-Arrhenius behavior. In this study, generalized vibrational frequencies based on harmonic approximation were used in the dynamics calculation. Because the low-frequency vibrational mode will behave as a free rotor at a high temperature,[33,34] the harmonic approximation may result in the curvature found above 600 K and shown in Figures 9−11. A recent study of some hydrogen abstraction reactions indicated that the observed curvature of plots of ln(k) vs 1/T may be due to changes in the enthalpy of activation that are caused by changes in the bond dissociation energy (BDE) of the breaking and making bonds with the temperature.[35] The location of the bottleneck determined by the variational TST calculation, which may incorporate temperature changes in the BDE, varies with the temperature. Table 2 summarizes the ICVT and ICVT/SCT rate constants in a temperature range of 200−400 K. The ICVT rate constants exhibit slightly non-Arrhenius behavior. Arrhenius plots between 200 and 300 K give activation energies of 2.4, 1.1, and 0.8 kcal/mol for $CH_3O + O_2$, $C_2H_5O + O_2$, and i-$C_3H_7O + O_2$ reactions, while those between 300 and 400 K give 2.6, 1.2, and 1.1 kcal/mol. Thus, non-Arrhenius behavior already appears in the variational TST process before the tunneling correction. Inclusion of the tunneling effects lowers the activation energies (1.1, 0.9, and 0.6 kcal/mol between 200 and 300 K; 1.6, 1.1, and 1.0 kcal/mol between 300 and 400 K for $CH_3O + O_2$, $C_2H_5O + O_2$, and i-$C_3H_7O + O_2$ reactions, respectively), because the tunneling effect has more significance at low temperatures. A comparison between ICVT and ICVT/SCT in Table 2 indicates that the tunneling effect is more significant in the order of i-$C_3H_7O + O_2$, $C_2H_5O + O_2$, and $CH_3O + O_2$ reactions. This is consistent with the fact that the absolute values of an imaginary frequency at the transition state (see Table 1), which is associated with the width of the energy barrier, increase in this order. Fits for the calculated rate constants to the three-parameter expression, $k = AT^n \exp(-E/T)$, in the temperature range T = 200−400 K lead to 2.02 ×

$10^{-23}T^{2.98}\exp(207/T)$, $1.41 \times 10^{-16}T^{0.80}\exp(-275/T)$, and $9.67 \times 10^{-20}T^{1.89}\exp(143/T)$ for the $CH_3O + O_2$, $C_2H_5O + O_2$, and $i\text{-}C_3H_7O + O_2$ reactions.

Conclusion

In this study, we provided reasonable rate constants in consistent agreement with experimental data through dynamics calculations of three alkoxy radical reactions with different environments of an abstractable hydrogen atom. The combination of high-level ab initio molecular orbital theory and variational TST with multidimensional semiclassical tunneling correction enables a direct comparison with the available experimental data without adjustment of the barrier height, as in some recent theoretical calculations, and thus demonstrates the usefulness of direct dynamics. We suggest that the electronic state of an ethoxy radical participating in a reaction with an oxygen molecule is both an A″ ground state and an A′ low-lying excited state, taking molecular orbitals and symmetry into consideration. The calculated rate constant for a $C_2H_5O + O_2$ reaction under such an assumption is in reasonable agreement with the experimental rate constant. The $i\text{-}C_3H_7O + O_2$ reaction shows a significant variational effect and can be treated only by VTST calculation. The reaction rate constants for $n\text{-}C_3H_7O$[6,8] and $2\text{-}C_4H_9O$[36,37] radical reactions with an oxygen molecule were shown to have lower temperature dependence (a negative temperature dependence for $2\text{-}C_4H_9O$) than the alkoxy radicals studied in this work. Dynamics calculations of these alkoxy radicals with an oxygen molecule may provide further insight into the substituent effect and the temperature dependence for the reaction rate constant, particularly at the low temperature in the troposphere. Alkoxy radical reactions with larger or more complicated substituent groups are now being investigated in our laboratory.

Acknowledgment. Our use of the computational facilities of the Tsukuba Advanced Computer (TAC) Center of the National Institute of Advanced Industrial Science and Technology (AIST) is gratefully acknowledged.

Supporting Information Available: Changes in geometrical parameters along the IRC at the UB3LYP/6-311G(d,p) and the CASSCF/TZV(2df,2p) levels and comparison between the UB3LYP PES and the G2M(RCC1) PES. This material is available free of charge via the Internet at http://pubs.acs.org.

References and Notes

(1) Lorenz, K.; Rhäsa, D.; Zellner, R.; Fritz, B. *Ber. Bunsen-Ges. Phys. Chem.* **1985**, *89*, 341.

(2) Wantuck, P. J.; Oldenborg, R. C.; Baughcum, S. L.; Winn, K. R. *J. Phys. Chem.* **1987**, *91*, 4653.

(3) Gutman, D.; Sanders, N.; Butler, J. E. *J. Phys. Chem.* **1982**, *86*, 66.

(4) Hartmann, D.; Karthäuser, J.; Sawerysyn, J. P.; Zellner, R. *Ber. Bunsen-Ges. Phys. Chem.* **1990**, *94*, 639.

(5) Zabarnick, S.; Heicklen, J. *Int. J. Chem. Kinet.* **1985**, *17*, 455.

(6) Fittschen, C.; Frenzel, A.; Imrik, K.; Devolder, P. *Int. J. Chem. Kinet.* **1999**, *31*, 860.

(7) Balla, R. J.; Nelson, H. H.; McDonald, J. R. *Chem. Phys.* **1985**, *99*, 323.

(8) Mund, Ch.; Fockenberg, Ch.; Zellner, R. *Ber. Bunsen-Ges. Phys. Chem.* **1998**, *102*, 709.

(9) Atkinson, R.; Baulch, D. L.; Cox, R. A.; Hampson, R. F., Jr.; Kerr, J. A.; Rossi, M. J.; Troe, J. *J. Phys. Chem. Ref. Data.* **1997**, *26*, 521.

(10) Jungkamp, T. P. W.; Seinfeld, J. H. *Chem. Phys. Lett.* **1996**, *257*, 15.

(11) Bofill, J. M.; Olivella, S.; Solé, A.; Anglada, J. M. *J. Am. Chem. Soc.* **1999**, *121*, 1337.

(12) Gonzalez, C.; Schlegel, H. B. *J. Phys. Chem.* **1990**, *94*, 5523.

(13) Miller, W. H.; Handy, N. C.; Adams, J. E. *J. Chem. Phys.* **1980**, *72*, 99.

(14) Mebel, A. M.; Morokuma, K.; Lin, M. C. *J. Chem. Phys.* **1995**, *103*, 7414.

(15) Schlegel, H. B. *J. Phys. Chem.* **1988**, *92*, 3075.

(16) Knowles, P. J.; Hampel, C.; Werner, H.-J. *J. Chem. Phys.* **1993**, *99*, 5219.

(17) Huzinaga, S. *J. Chem. Phys.* **1965**, 42, 1293.

(18) Dunning, T. H. *J. Chem. Phys.* **1971**, 55, 716.

(19) Frisch, M. J.; Trucks, G. W.; Schlegel, H. B.; Scuseria, G. E.; Robb, M. A.; Cheeseman, J. R.; Zakrzewski, V. G.; Montgomery, J. A., Jr.; Stratmann, R. E.; Burant, J. C.; Dapprich, S.; Millam, J. M.; Daniels, A. D.; Kudin, K. N.; Strain, M. C.; Farkas, O.; Tomasi, J.; Barone, V.; Cossi, M.; Cammi, R.; Mennucci, B.; Pomelli, C.; Adamo, C.; Clifford, S.; Ochterski, J.; Petersson, G. A.; Ayala, P. Y.; Cui, Q.; Morokuma, K.; Malick, D. K.; Rabuck, A. D.; Raghavachari, K.; Foresman, J. B.; Cioslowski, J.; Ortiz, J. V.; Stefanov, B. B.; Liu, G.; Liashenko, A.; Piskorz, P.; Komaromi, I.; Gomperts, R.; Martin, R. L.; Fox, D. J.; Keith, T.; Al-Laham, M. A.; Peng, C. Y.; Nanayakkara, A.; Gonzalez, C.; Challacombe, M.; Gill, P. M. W.; Johnson, B. G.; Chen, W.; Wong, M. W.; Andres, J. L.; Head-Gordon, M.; Replogle, E. S.; Pople, J. A. *Gaussian 98*, revision A.7; Gaussian, Inc.: Pittsburgh, PA, 1998.

(20) Werner, H.-J.; Knowles, P. J. with contributions from Amos, R. D.; Bernhardsson, A.; Berning, A.; Celani, P.; Cooper, D. L.; Deegan, M. J. O.; Dobbyn, A. J.; Eckert, F.; Hampel, C.; Hetzer, G.; Korona, T.; Lindh, R.; Lloyd, A. W.; McNicholas, S. J.; Manby, F. R.; Meyer, W.; Mura, M. E.; Nicklass, A.; Palmieri, P.; Pitzer, R.; Rauhut, G.; Schütz, M.; Stoll, H.; Stone, A. J.; Tarroni, R.; Thorsteinsson, T. *MOLPRO 2000.1*; University of Birmingham: Birmingham, AL, 1997.

(21) Schmidt, M. W.; Baldridge, K. K.; Boatz, J. A.; Elbert, S. T.; Gorden, M. S.; Jensen, J. H.; Koseki, S.; Matsunaga, M.; Nguyen, K. A.; Su, S.; Windus, T. L.; Dupuis, M.; Montgomery, J. A. *J. Comput. Chem.* **1993**, *14*, 1347.

(22) Truhlar, D. G.; Isaacson, A. D.; Garrett, B. C. *The Theory of Chemical Reaction Dynamics*; Baer, M., Ed.; CRC Press: Boca Raton, FL, 1985; Vol. 4, p 65.

(23) Garrett, B. C.; Truhlar, D. G. *J. Chem. Phys.* **1979**, *83*, 1052.

(24) Corchado, J. C.; Chuang, Y.-Y.; Fast, P. L.; Villà, J.; Hu, W.-P.; Liu, Y.-P.; Lynch, G. C.; Nguyen, K. A.; Jackels, C. F.; Melissas, V. S.; Lynch, B. J.; Rossi, I.; Coitiño, E. L.; Fernandez-Ramos, A.; Steckler, R.; Garrett, B. C.; Isaacson, A. D.; Truhlar, D. G. *POLYRATE*; version 8.5.1; University of Minnesota: Minneapolis, MN, 2000.

(25) Foster, S. C.; Hsu, Y.-C.; Damo, C. P.; Liu, X.; Kung, C.-Y.; Miller, T. A. *J. Phys. Chem.* **1986**, *90*, 6766.

(26) Ramond, T. M.; Davico, G. E.; Schwartz, R. L.; Lineberger, W. C. *J. Chem. Phys.* **2000**, *112*, 1158.

(27) Tan, X. Q.; Williamson, J. M.; Foster, S. C.; Miller, T. A. *J. Phys. Chem.* **1993**, *97*, 9311.

(28) Curtiss, L. A.; Lucas, D. J.; Pople, J. A. *J. Chem. Phys.* **1995**, *102*, 3292.

(29) Hammond, G. S. *J. Am. Chem. Soc.* **1955**, *77*, 334.

(30) Truong, T. N.; Truhlar, D. G. *J. Chem. Phys.* **1990**, *93*, 1761.

(31) Pacey, P. D. *J. Chem. Educ.* **1981**, *58*, 612.

(32) Sekušak, S.; Cory, M. G.; Bartlett, R. J.; Sabljiæ, A. *J. Phys. Chem. A* **1999**, *103*, 11394.

(33) Ayala, P. Y.; Schlegel, H. B. *J. Chem. Phys.* **1998**, *108*, 2314.

(34) Chuang, Y.-Y.; Truhlar, D. G. *J. Chem. Phys.* **2000**, *112*, 1221.

(35) Zavitsas, A. A. *J. Am. Chem. Soc.* **1998**, *120*, 6578.

(36) Deng, W.; Wang, C.; Katz, D. R.; Gawinski, G. R.; Davis, A. J.; Dibble, T. S. *Chem. Phys. Lett.* **2000**, *330*, 541.

(37) Deng, W.; Davis, A. J.; Zhang, D. L.; Katz, D. R.; Dibble, T. S. *J. Phys. Chem. A* **2001**, *105*, 8985.